A case study of multi-structure turbulence: uniformly sheared flow distorted by a grid

Jovan Nedić

Department of Mechanical Engineering
McGill University, Canada
jovan.nedic@mcgill.ca

Stavros Tavoularis

Department of Mechanical Engineering
University of Ottawa, Canada
stavros.tavoularis@uottawa.ca

ABSTRACT

The fine and large–scale properties in spatially developing uniformly sheared flow (USF) and USF distorted by a square–mesh grid was examined experimentally using one– and two–point, two–component hot–wire anemometry. We confirmed previous findings that USF has an intermediate region where the dissipation parameter scales with the local turbulent Reynolds number as $C_\varepsilon \propto \mathrm{Re}_\lambda^{-0.6}$ and a far downstream region, where $C_\varepsilon \approx$ const.. The insertion of a grid across the USF resulted in the creation of *multi-structure* turbulence and a permanent reduction of kinetic energy and length scales of the turbulence. Near the grid the dissipation parameter scaled as $C_\varepsilon \propto \mathrm{Re}_\lambda^{-1}$, as in decaying grid turbulence, despite the opposite evolution rates of the kinetic energy (and Re_λ) in the two flows. The turbulence fine structure within this multi–structure region was unaffected significantly by the grid, whereas the large–scale anisotropy was markedly changed by the grid. Second–order structure functions, normalised by Kolmogorov scales, collapsed in the viscous sub–range, as well as for the largest measured separations. Within the inertial sub–range, however, the effects of grid insertion were measurable.

INTRODUCTION

Of central importance in turbulence research is the Richardson-Kolmogorov energy cascade postulate, which predicts the existence of a $-5/3$ range in the kinetic energy spectrum (Tennekes & Lumley, 1972; Pope, 2000). This theory, as well as derivations of far-field scaling laws for canonical turbulent flows (Townsend, 1980), have uniformly assumed that the dissipation parameter $C_\varepsilon = \varepsilon L/(2k/3)^{3/2}$ (k is the turbulent kinetic energy per unit mass, ε is its dissipation rate and L is the integral length scale) is approximately constant (Batchelor, 1953). The same assumption is also pivotal for the derivation of turbulence models used to enforce closure of the Reynolds-averaged Navier-Stokes (RANS) equations (Launder & Spalding, 1972), subgrid-scale models for large-eddy simulations (LES) (Meneveau & Katz, 2000; Piomelli, 2014), expressions predicting turbulent dispersion of scalars (Tavoularis & Nedić, 2017) as well as for the estimation of computer resources for direct numerical simulations (DNS) (Launder & Spalding, 1972; Vassilicos, 2015). The constancy of C_ε is in turn based on the assumption that the turbulence structure is well developed and evolves in a self-similar manner. Nevertheless, most natural and technological flows are unlikely ever to reach a state of full self-similarity, or may do so far away from their origins, beyond the domain of practical interest. The formulation of a universal theory of developing turbulence is an unattainable goal, not only because of the structural differences among different types of turbulence but also because even a flow on its way to full development may undergo several stages, in each of which the dynamics of development of different parameters could be different. In fact, there is currently a growing body of evidence that specific canonical turbulent flows have not only a state in which $C_\varepsilon \approx$ const. along mean streamlines, but also one or more other states in which this parameter may be scaled by local conditions. More specifically, C_ε has been expressed as a power function $C_\varepsilon \propto \mathrm{Re}_\lambda^\alpha$ of the local Reynolds number $\mathrm{Re}_\lambda = (2k/3)^{1/2}\lambda/\nu$, in which ν is the kinematic viscosity and λ is the Taylor microscale, related to the other parameters by $\lambda = \sqrt{10\nu k/\varepsilon}$. Flows with known power-law regions include grid turbulence (Vassilicos, 2015), axisymmetric wakes (Nedić *et al.*, 2013), uniformly sheared flows (USF) (Nedić & Tavoularis, 2016) and constant-pressure turbulent boundary layers (Nedić *et al.*, 2017).

A common characteristic of earlier studies has been that their interest focussed on the transformation of the structure of a specific canonical flow from an initial, apparatus-dependent state to its $C_\varepsilon \approx$ const. state, in which all turbulence properties, including k, ε and L grew at commensurate rates. Although initial states generated by apparatus with different specifications were examined in some grid turbulence studies, none of the previously mentioned references describes a deliberate attempt to distort an already developed structure in a radical manner. The objective of the present research is to examine and explain the structural transformation of turbulence from one prescribed state to another. The rationale and strategic approach for achieving this goal are as follows.

Let us consider a canonical flow, which has a natural $C_\varepsilon \approx$ const. state and which was allowed to reach this state, so that its structure was essentially free of apparatus effects. Then, let us introduce a disturbance into this flow, which is strong enough to impose its own preferential turbulence structure in its vicinity, but whose effects would eventually decay downstream so that the undistorted structure of the original canonical flow would be recovered, although not necessarily without permanent changes in the levels of the various turbulence properties. Now, there is a flow region in which the turbulence structure would undergo a *metamorphosis* from a disturbance-dominated state to a disturbance-free state. This would be a region of *multi-structure* turbulence, namely one in which at least two kinds of dominant eddies exist and compete for contributing to the local averages at the energy-containing level, but also possibly in the fine structure. As a first step towards understanding this transformation mechanism, it seems advisable to examine idealised basic flows and disturbances. Our respective choices were USF and grid-generated turbulence. Both of these flows have been studied extensively and have well known structures that are very different from each other. In particular, USF has a highly anisotropic turbulent stress tensor, well-organised coherent structures and a turbulent kinetic energy that grows exponentially with increasing distance from its origin, whereas grid turbulence is nearly isotropic and decays. Consequently, we expect to have well-defined and very distinct initial and final states for the multi-structure flow region.

The implications of this work and its future extensions could be far reaching, as the vast majority of practical flows are multi-structure. Abundant examples can be found in many industrial, aerospace and transportation systems, but also in the atmosphere, oceans and other bodies of water, and in biological contexts (*e.g.*, the cardiovascular and pulmonary systems). The theoretical treatment and computational modelling of such flows is beyond the capabilities of the Richardson-Kolmogorov postulate and related classical turbulence concepts and this work will hopefully contribute towards developing alternative analyses and models.

APPARATUS AND INSTRUMENTATION

The wind tunnel facility and shear generating apparatus (Fig. 1) were the same as those in our previous study (Nedić & Tavoularis, 2016), with one modification: the far downstream walls of the test section were adjusted in order to maintain a constant pressure, thus extending the range of meaningful measurements beyond previously possible values. Uniform mean shear was generated by a shear generator, followed by a flow straightener, both of which comprised 12 channels with a spacing of M = 25.4 mm. One of three square–mesh grids was inserted across the flow at a downstream distance $x_1 = 4.5h$, where $h = 0.305$ m is the height of the test section. The three grids included a perforated plate (RG18) with a mesh size $M_g = 18.00$ mm and a solidity of 0.25 and two screens made of woven wire (RG13 and RG3) with mesh sizes 12.70 and 3.18 mm and a solidity of 0.29. All grids were chosen as to introduce a relatively mild, small–scale distortion to the USF turbulence. In particular, the mesh sizes of RG18 and RG13 were somewhat smaller than the value 21 mm of the integral length scale of undistorted USF at the location of grid insertion, whereas that of RG3 was much smaller.

All measurements were made using constant temperature hot–wire anemometers. Single–point measurements of the streamwise and transverse velocity components were made with a custom–made device, which included a cross–wire probe with sensor lengths of 0.85 mm and a normal sensor with a length of 0.5 mm, so that two sets of measurements of streamwise properties could be obtained simultaneously and compared to each other. Two–point measurements were made with two cross-wire probes, each of which was traversed independently from the other in the x_2 direction. The diameter of all sensors was 2.5 μm and the distance between adjacent sensors was 0.5 mm. Unless otherwise stated, turbulent statistics presented below were obtained with the three–sensor device. Streamwise derivatives were estimated from temporal ones with the use of Taylor's frozen flow approximation. The rate of turbulent kinetic energy dissipation was calculated as $\varepsilon = 15\nu\overline{(\partial u_1/\partial x_1)^2}$ and the streamwise Taylor microscale as $\lambda = (15\nu u_1'^2/\varepsilon)^{1/2}$, where u_1' is the standard deviation of the streamwise velocity fluctuations. The streamwise integral scales $L_{11,1}$ and $L_{22,1}$ were computed by integrating the corresponding temporal autocorrelation functions to their first zeros and employing Taylor's frozen flow approximation, whereas the transverse integral length scales $L_{11,2}$ and $L_{22,2}$ were determined by integrating the corresponding two-point correlation coefficients (measured by the two cross–wire probes) to their first zeros. Finally, the dissipation parameter was estimated as $C_\varepsilon = \varepsilon L_{11,1}/u_1'^3$.

THE MEAN AND TURBULENT FIELDS

Fig. 2 shows the streamwise evolutions of $\overline{u_1^2}$, the shear stress correlation coefficient $\rho = -\overline{u_1 u_2}/u_1' u_2'$, $L_{11,1}$, Re_λ and C_ε for the undistorted and distorted cases. As expected, $\overline{u_1^2}$ grew exponentially in undistorted USF (Tavoularis, 1985), and decayed within a region downstream of each grid before eventually recovering an exponential growth with approximately the same exponent as in undistorted flow. The presence of a grid introduced a permanent loss of $\overline{u_1^2}$, which increased with decreasing M_g. It is noted that the region very close to the grid, where the turbulence is strongly inhomogeneous and there is local production by an alternating mean shear is not of interest in this work. ρ, which is a measure of the Reynolds stress tensor anisotropy, was reduced from a value near 0.4 in undistorted USF to much lower values near a grid, but eventually recovered its USF value in all cases. $L_{11,1}$ was reduced drastically by the introduction of a grid, but in all cases it recovered an exponential growth rate that was comparable to that in undistorted USF. λ (not shown here) was constant for all cases for $x_1 \geq 9h$ and increased with decreasing M_g. Re_λ was reduced significantly following the insertion of a grid and, although its rate of increase eventually matched the undistorted USF level, its local values remained lower. All four flows had significant upstream regions in which C_ε underwent a large stepwise increase behind a grid, but then decreased rapidly and settled at approximately the same constant value as in undistorted USF. One–dimensional energy spectra, not shown here, had identifiable inertial sub–ranges, which became broader and had a slope that tended towards -5/3 as the local Reynolds number increased. In summary, all measurements indicate that the turbulence within a range of distances from any of the three grids was multi–structure and had features that were intermediate between those in USF and grid–generated turbulence. Beyond this multi–structure range, the turbulence relaxed to the undistorted USF self–similar state, in which distortion by the grid persisted only in the form of a permanent reduction in the values of k and $L_{11,1}$.

Fig. 3 shows C_ε *vs.* Re_λ. It is evident that all three distorted USF reached states in which $C_\varepsilon \approx$ const., with all asymptotic values being in proximity of the value in undistorted USF. This figure demonstrates once again that the local Re_λ was significantly lower in distorted than undistorted USF. All four flows had significant upstream regions in which $C_\varepsilon \approx \mathrm{Re}_\lambda^\alpha$ with $\alpha < 0$. In the undistorted USF, this corresponded to a multi-structure region, in which apparatus–generated structures coexisted with shear–generated structures and where $\alpha \approx -0.6$, in agreement with our previous finding (Nedić & Tavoularis, 2016). The three distorted USF also had such regions, albeit with $\alpha \approx -1$. This value is remarkably identical to the one found near the grid in purely grid-generated turbulence (Vassilicos, 2015), but these two types of flows have a very important difference: in grid turbulence Re_λ decreases downstream, whereas in grid-distorted USF it increases. This observation implies that the distorted USF turbulence is not identical to grid turbulence but truly multi–structure. It follows further that a power law with $\alpha \approx -1$ is not necessarily an empirical fit to a specific type of turbulence. Of course, the ubiquity of a region with $\alpha \approx -1$ is contradicted by the undistorted USF value of -0.6. Fig. 3 also shows that in all cases C_ε reached a minimum and then increased to reach its asymptotic value. In the case of undistorted USF, this region was sufficiently long to be fitted with a power law having $\alpha = 1$, which agrees in sign but differs in value from our previous (Nedić & Tavoularis, 2016) finding of $\alpha = 0.5$. This difference can be possibly attributed to small differences in the pressure gradient in that region of the flow, as a result of side wall adjustment for the purpose of boundary layer compensation, as well as to the large uncertainty of power law fitting to the comparatively few data values that were available in that region. As the distorted USF flows also have ascending C_ε regions, we cannot easily dismiss the occurrence of some sort of structural overshooting, but our data are not sufficient for a conclusive investigation of this issue, which we delegate to future research.

LARGE–SCALE ANISOTROPY

We have previously (Nedić & Tavoularis, 2016) associated the presence of a region with a variable C_ε in undistorted USF with the observation that $L_{11,1}$ approaches its asymptotic growth rate further downstream than where k and ε approach theirs. In this section, we report measurements of $L_{11,1}$ in grid-distorted USF, as well as measurements of three additional integral length scales, $L_{22,1}, L_{11,2}$ and $L_{22,2}$, normalised by the local $L_{11,1}$, both in undistorted and grid-distorted USF. The first two subscripts in these scales indicate

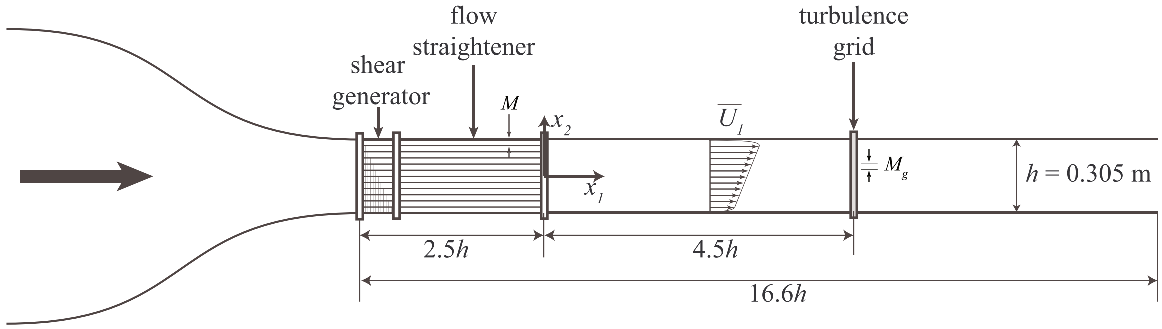

Figure 1. Schematic diagram of the wind tunnel, showing the shear–generating apparatus, the co–ordinate system and the location of the grid.

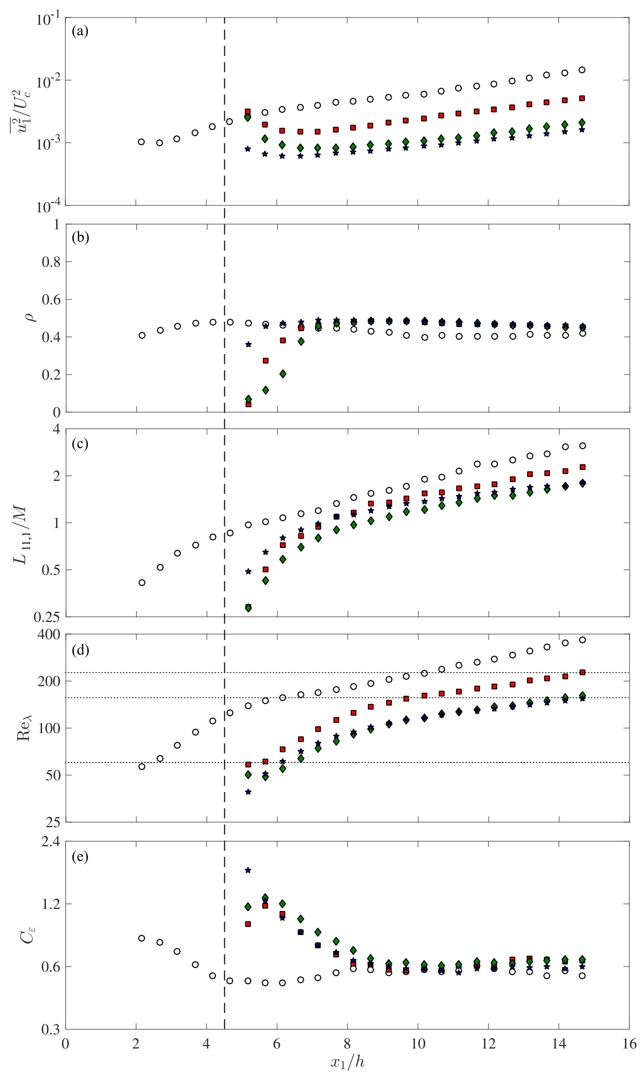

Figure 2. Streamwise evolutions of (a) the variance of the streamwise velocity fluctuations, (b) the shear stress correlation coefficient, (c) the streamwise integral length scale of the streamwise fluctuating velocity, (d) the turbulent Reynolds number and (e) the dissipation parameter for undistorted USF (circles) and USF distorted by RG18 (red squares), RG13 (green diamonds) and RG3 (blue stars); all measurements were made along the test section centreline, where the mean velocity was $U_c = 8.1$ m/s.

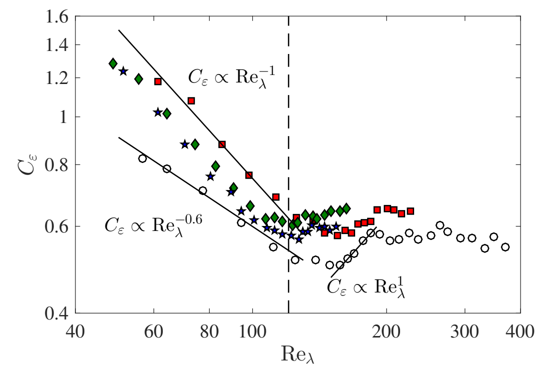

Figure 3. Dissipation parameter plotted *vs.* the turbulence Reynolds number; symbols as in Fig. 2; dashed line marks the value of Re_λ in undistorted USF at the location of grid insertion.

the direction of the velocity component, whereas the third one indicates the direction of spatial separation. The transverse two-point correlations used to determine $L_{11,2}$ and $L_{22,2}$ were measured by increasing the probe separation such that either probe was equally distant from the test section centreline. The ratios of these scales may serve as measures of the anisotropy of large–scale motions; as reference, in isotropic turbulence, $L_{22,1}/L_{11,1} = L_{11,2}/L_{11,1} = 1/2$ and $L_{22,2}/L_{11,1} = 1$ (Batchelor, 1953).

In Fig. 4 we show the streamwise evolution of the measured integral length scale ratios $L_{22,1}/L_{11,1}$, $L_{11,2}/L_{11,1}$ and $L_{22,2}/L_{11,1}$ for the undistorted USF case and the three distorted cases. First, let us examine the undistorted USF results. All scale ratios increased monotonically with downstream distance up to $x_1/h \approx 11$ and then appeared to settle at values that were much lower than the isotropic levels. The latter observation is hardly a surprise, because the strong anisotropy of USF structure is well known. What is novel is the fact that this anisotropy takes a long distance to reach self-similarity and evolves over some distance even after C_ε has settled at a constant level. The asymptotic value of $L_{22,2}/L_{11,1}$ was about one third of its isotropic counterpart, which is compatible with a previous observation that dominant coherent structures in USF are stretched much more in the streamwise direction than in the transverse one (Vanderwel & Tavoularis, 2011). The only other available measurements of integral length scale ratios in USF are those by Vanderwel & Tavoularis (2014), made in a water tunnel with the use of stereoscopic particle image velocimetry. Those measurements have values that are larger than the present asymptotic values but were taken at a location that corresponded to the early stages of the present USF where our values were larger than the asymptotic ones as well.

As shown in Fig. 2c, insertion of a grid resulted in a local, but also a permanent, reduction of $L_{11,1}$ and the reduction became stronger with decreasing grid mesh size. Figs. 4b-d show the ef-

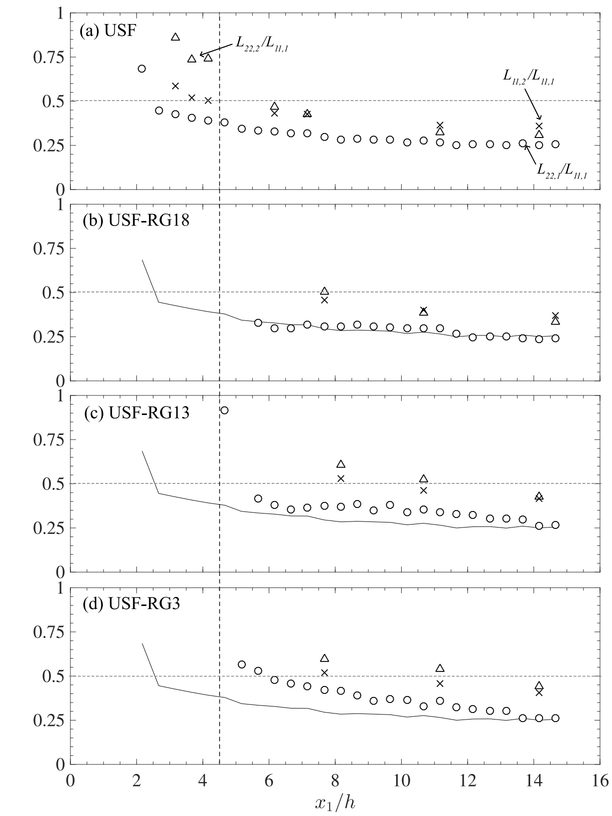

Figure 4. Streamwise evolutions of integral length scale ratios $L_{22,1}/L_{11,1}$ (circles), $L_{11,2}/L_{11,1}$ (cross) and $L_{22,2}/L_{11,1}$ (triangle) for (a) undistorted USF and USF distorted by (b) RG18, (c) RG13 and (d) RG3. Solid line in (b)-(d) is $L_{22,1}/L_{11,1}$ in the undistorted USF case. Vertical dash lines mark the grid insertion location.

fect of grid insertion on the length scale ratio. One may plausibly anticipate that the grid would introduce an isotropisation effect in its vicinity. Somewhat surprisingly, RG18 shows little evidence for such an effect within the range of the present measurements, which did not extend very close to the grid. As far as large–scale anisotropy is concerned, RG18 appears to be entirely passive. In contrast, RG13, which has an only slightly smaller mesh than RG18 (but also a higher solidity and a different design) had a clearly visible isotropisation effect, with the scale ratios relaxing to the undistorted USF levels only at the very end of the test section. A comparable isotropisation effect was also observed for RG3.

THE FINE STRUCTURE

In this section, we investigate the evolution of the fine structure of undistorted and grid-distorted USF. First we examine the level of local anisotropy using as indicators the following ratios of the variances of the few measurable velocity derivatives

$$K_1 = 2\frac{\overline{(\partial u_1/\partial x_1)^2}}{\overline{(\partial u_2/\partial x_1)^2}},\ K_2 = 2\frac{\overline{(\partial u_2/\partial x_2)^2}}{\overline{(\partial u_1/\partial x_2)^2}},\ K_3 = 2\frac{\overline{(\partial u_1/\partial x_1)^2}}{\overline{(\partial u_1/\partial x_2)^2}}. \quad (1)$$

All of these ratios should all be unity in locally isotropic turbulence. The measured four derivative variances are among the 15 terms that sum up to ε. For consistency, we measured all four derivatives with the dual cross-wire probe. We estimated streamwise derivatives from temporal derivatives *via* Taylor's frozen flow approximation and interpolated between values measured by the two probes to estimate the corresponding value on the test section centreline. In the

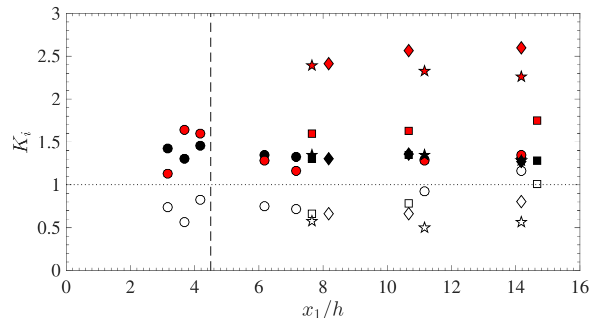

Figure 5. Streamwise evolutions of the local anisotropy indicators K_1 (black symbols), K_2 (red symbols) and K_3 (open symbols) for undistorted USF (circles) and USF distorted by RG18 (squares), RG13 (diamonds) and RG3 (stars).

cases for which measurements could be obtained with the single sensor, the results were found to be very close to the ones reported here. Variances of transverse derivatives were estimated by extrapolating variances of differences between values measured by the two probes to a zero separation; the minimum separation distance between the centroids of these probes was 1.5 mm. These results, especially the values of $\overline{(\partial u_2/\partial x_2)^2}$, are subjected to uncertainty due to the limited spatial resolution and aerodynamic interference (Valente & Vassilicos, 2014; Zhu & Antonia, 1996). In view of this limitation, the significance of this discussion is mainly qualitative.

Figure 5 shows measurements of K_1, K_2 and K_3. All properties had considerable scatter, but the trends allow us to make some general observations. K_1 took values of about 1.3 for all configurations, undistorted and distorted, and throughout the range of measurements; this value is consistent with previous measurements in undistorted USF (Tavoularis & Corrsin, 1981). K_3 also was nearly constant, irrespectively of location and configuration. The present value $K_3 \approx 0.75$ was consistent with the one reported by Ferchichi & Tavoularis (2000) in the same facility using parallel sensors 0.5 mm apart, but higher than the value 0.45 reported by Tavoularis & Corrsin (1981). Finally, K_2, for which we found no previous measurements, also appeared to be independent of location within the test range, but its value seemed to be affected significantly and permanently by the insertion of a grid. For comparative purposes, K_2 was roughly 1.3 in undistorted USF, 1.65 behind RG18 and 2.5 behind either RG13 or RG3. Such changes appear to be higher than the anticipated uncertainty level and seem to indicate that it is mainly $\overline{(\partial u_2/\partial x_2)^2}$ that is affected by a grid. In any case, the near constancy of all indicators implies that the fine structure became adjusted very fast to its asymptotic state.

To gain a deeper understanding of the evolution of the fine structure, we now investigate the evolutions of the normalised second and third order structure functions, *i.e.*, $C_{n1} = \overline{(\delta u_1)^n}/(r\varepsilon)^{n/3} = \overline{[u_1(x_1+r) - u_1(x_1)]^n}/(r\varepsilon)^{n/3}, n = 2,3$. Kolmogorov's hypotheses imply that these functions would be universal in the inertial and viscous subranges, provided that the local turbulence Reynolds number Re_λ is sufficiently large. Figure 6 shows the centreline evolution of these two structure functions in undistorted USF, measured with the single–sensor probe and the Taylor approximation. The data at all streamwise positions only collapsed within a range of small separations ($1 < r/\eta < 10$; η is the Kolmogorov microscale), but the collapse region became wider with increasing streamwise distance. This is hardly surprising, because in USF increasing streamwise distance also corresponds to an increasing Re_λ, and therefore an increasing width of the inertial subrange; within this subrange, $C_{21} \approx 2.2$, in line with previous findings (Ferchichi & Tavoularis, 2000; Boratav & Pelz, 1997). The

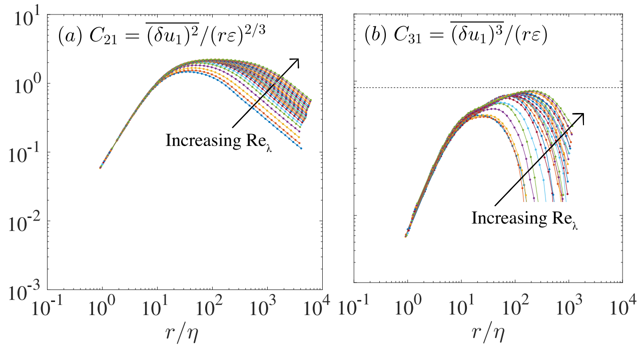

Figure 6. Streamwise evolutions of the normalised second (a) and third (b) order streamwise structure functions for the undistorted USF case. The horizontal line in (b) marks C_{31} = 4/5.

third order structure function tended towards developing a region where it would attain the universal value -4/5, although it fell short of reaching such a state at even the largest Re_λ considered.

The scaling of the structure functions is known to be Reynolds number dependent (Ferchichi & Tavoularis, 2000; Garg & Warhaft, 1998). Therefore, for a meaningful comparison between these functions in disturbed and undisturbed USF, we compared a few cases of undistorted and grid-distorted USF at locations with the same value of Re_λ. The relative streamwise locations of these measurements can be seen in Fig. 2d and some important values are listed in Table 1. The lowest Reynolds number, $Re_\lambda \approx 60$, was selected as it falls within the multi–structure region behind the grids, whereas the highest one, $Re_\lambda = 366$, which was achieved at the test section end for undistorted USF only, will be used as reference for comparing the shapes of the transfer functions.

Table 1. Turbulent scale ratios and dissipation parameter at three turbulent Reynolds numbers in undistorted and grid–distorted USF.

Flow	Re_λ	λ/η	$L_{11,1}/\eta$	C_ε	ρ	x_1/h
USF	56	15	46	0.83	0.41	2.2
	163	25	142	0.52	0.45	6.7
	224	30	258	0.59	0.41	10.2
	366	38	507	0.55	0.42	14.7
USF-RG18	59	15	57	0.95	0.1	5.2
	161	25	156	0.58	0.48	10.2
	227	30	303	0.68	0.45	14.7
USF-RG13	64	15	64	1.21	0.39	6.2
	160	25	183	0.69	0.36	14.2
USF-RG3	60	15	62	1.02	0.47	6.2
	160	25	164	0.62	0.46	14.7

In Fig. 7 we show the normalised second order structure functions C_{21} for the four examined configurations and any of four turbulent Reynolds numbers for which measurements were available. The following interesting observations can be tentatively based on

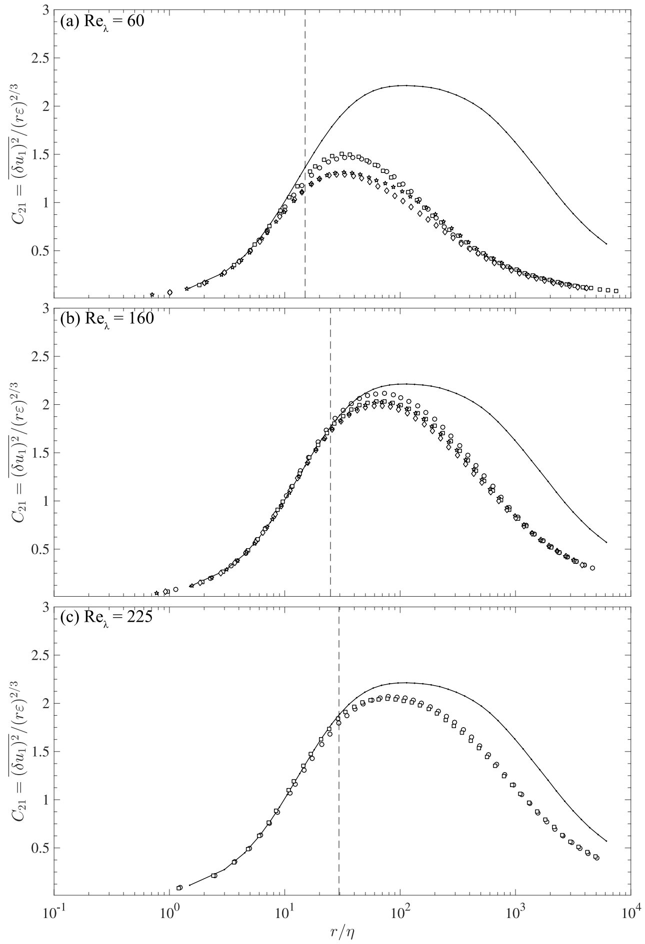

Figure 7. Normalised second order structure functions for Re_λ = 80 (a), 160 (b) and 225 (c) in undistorted USF (circles) and USF distorted by RG18 (squares), RG13 (diamonds) and RG3 (stars). Note that in (c) we only show data for the undistorted USF and USF distorted by RG18. The solid line in all plots corresponds to results in undistorted USF for Re_λ = 366, which was the largest achieved. Vertical dashed lines mark the Taylor microscale.

these plots.

1. For all three Reynolds numbers, the structure functions for both distorted and undistorted cases collapsed within the separation range $r \lesssim 10\eta$, which extended to values that were considerably lower than the Taylor microscale and so must represent mostly the viscous subrange. This means that any distortion of motions in this range caused by the grid decayed very quickly downstream.
2. Surprisingly, the structure functions for both distorted and undistorted cases also collapsed for very large separations ($r \gtrsim 80\eta$). This seems to imply that any distortion imposed by the grid on the USF coherent structure streamwise extent, when normalised by the local dissipation rate, was negligible. In other words, the use of the dissipation rate as a scale was successful in collapsing the data for these large–scale motions, although the actual integral length scales suffered a permanent reduction behind the grids.
3. It is only in the intermediate range of separations, which presumably overlaps largely with the inertial subrange, that distortion effects were measurable. The differences among different configurations decreased with increasing Reynolds number, as

expected in consideration of the fact that multi–structure turbulence tended to relax towards the USF structure. Separating the effects of the three different grids is rather complex. It seems that, for $\mathrm{Re}_\lambda \approx 60$ and possibly also for $\mathrm{Re}_\lambda \approx 160$, the effects of the two smaller grids were stronger than those of RG18, although the larger grid caused a much stronger structural distortion, as, for example, evidenced by the very small value of ρ at $\mathrm{Re}_\lambda \approx 60$. It is possible that the RG18 results contain effects of inhomogeneity and/or vortex shedding from the grid bars. Moreover, the ratio of the actual dissipation rate and its estimate from streamwise measurements in multi–structure turbulence would likely be different from that in undistorted USF.

CONCLUSIONS

Compared to our previous report (Nedić & Tavoularis, 2016), the present study extended the range of measurements in developing USF. Multi–structure turbulence was created by the insertion of one of three small–mesh grids across the USF. This resulted in substantial changes of the levels of all turbulence parameters, including the turbulent kinetic energy and its dissipation rate, as well as the various length scales of turbulence. Whereas the levels of all parameters retained permanent reductions, their evolution rates eventually relaxed to the undistorted USF values. Grid–distorted USF was found to have a region near the grid where $\alpha = -1$, as in purely grid–generated turbulence, although, unlike in conventional grid turbulence, in the present case Re_λ was an increasing function of distance from the grid.

The effect of grid insertion on the turbulent motions of all scales were also investigated. Within the reported range of measurements, no discernible changes were observed in the local anisotropy and in the second–order structure functions. On the other hand, there was a noticeable change in the large–scale anisotropy ratios. The ratio $L_{22,1}/L_{11,1}$ was as low as 0.3 in the undisturbed USF case, which confirms that previously identified, dominant, hair–pin–shaped coherent structures are more elongated in the streamwise direction than in the transverse one.

Second–order structure functions in undistorted and grid–distorted USF at comparable Re_λ collapsed in the respective viscous sub–range as well as for the largest investigated separations, when normalised by Kolmogorov scales. In contrast, within the inertial sub–range, this structure function was affected by grid insertion in the vicinity of the grid.

Financial support by the Natural Sciences and Engineering Research Council of Canada (NSERC) is gratefully acknowledged.

REFERENCES

Batchelor, G. K. 1953 *The Theory of Homogeneous Turbulence*. Cambridge, UK: Cambridge University Press.

Boratav, O. N. & Pelz, R. B. 1997 Structures and structure functions in the inertial range of turbulence. *Phys. Fluids* **9** (5), 1400–1415.

Bos, W. J. T. & Rubinstein, R. 2017 Dissipation in unsteady turbulence. *Phys. Rev. Fluids* **2** (2).

Bos, W. J. T., Shao, L. & Bertoglio, J.-P. . 2007 Spectral imbalance and the normalized dissipation rate of turbulence. *Phys. Fluids* **19** (4), 045101.

Ferchichi, M. & Tavoularis, S. 2000 Reynolds number effects on the fine structure of uniformly sheared turbulence. *Phys. Fluids* **12** (11), 2942.

Garg, S. & Warhaft, Z. 1998 On the small scale structure of simple shear flow. *Phys. Fluids* **10** (3), 662–673.

Goto, S. & Vassilicos, J.C. C. 2015 Energy dissipation and flux laws for unsteady turbulence. *Phys. Lett. A* **379** (16-17), 1144–1148.

Goto, S. & Vassilicos, J. C. 2016 Unsteady turbulence cascades. *Phys. Rev. E* **94** (5-1), 053108.

Launder, B. E. & Spalding, D. B. 1972 *Lectures in mathematical models of turbulence*. New York: Academic Press.

Meneveau, C. & Katz, J. 2000 Scale-invariance and turbulence models for large-eddy simulation. *Annu. Rev. Fluid Mech.* **32** (1), 1–32.

Nedić, J. & Tavoularis, S. 2016 Energy dissipation scaling in uniformly sheared turbulence. *Phys Rev E* **93** (3), 033115.

Nedić, J., Tavoularis, S. & Marusic, I. 2017 Dissipation scaling in constant-pressure turbulent boundary layers. *Phys. Rev. Fluids* **2** (3).

Nedić, J., Vassilicos, J. C. & Ganapathisubramani, B. 2013 Axisymmetric turbulent wakes with new nonequilibrium similarity scalings. *Phys. Rev. Lett.* **111** (14).

Piomelli, U. 2014 Large eddy simulations in 2030 and beyond. *Phil. Trans R. Soc. A* **372** (2022), 20130320.

Pope, S. B. 2000 *Turbulent flows*. IOP Publishing.

Tavoularis, S. 1985 Asymptotic laws for transversely homogeneous turbulent shear flows. *Phys. Fluids* **28** (3), 999.

Tavoularis, S. & Corrsin, S. 1981 Experiments in nearly homogeneous turbulent shear flow with a uniform mean temperature gradient. part 2. the fine structure. *J. Fluid Mech.* **104**, 349–367.

Tavoularis, S. & Nedić, J. 2017 Taylorian diffusion in mildly inhomogeneous turbulence. *Int. J. Heat Fluid Flow* .

Tennekes, H. & Lumley, J. L. 1972 *A first course in turbulence*. MIT press.

Townsend, A. A. 1980 *The structure of turbulent shear flow*. Cambridge university press.

Valente, P. C., Onishi, R. & da Silva, C. B. 2014 Origin of the imbalance between energy cascade and dissipation in turbulence. *Phys. Rev. E* **90** (2), 023003.

Valente, P. C. & Vassilicos, J. C. 2014 The non-equilibrium region of grid-generated decaying turbulence. *J. Fluid Mech.* **744**, 5–37.

Vanderwel, C. & Tavoularis, S. 2011 Coherent structures in uniformly sheared turbulent flow. *J. Fluid Mech.* **689**, 434–464.

Vanderwel, C. & Tavoularis, S. 2014 Measurements of turbulent diffusion in uniformly sheared flow. *J. Fluid Mech.* **754**, 488–514.

Vassilicos, J. C. 2015 Dissipation in turbulent flows. *Annu. Rev. Fluid Mech.* **47** (1), 95–114.

Zhu, Y. & Antonia, R. A. 1996 The spatial resolution of hot-wire arrays for the measurement of small-scale turbulence. *Meas. Sci. Tech.* **7** (10), 1349.